PAPER

Attosecond polarization control in atomic RABBITT-like experiments assisted by a circularly polarized laser

IOP Publishing Journal of Physics B: Atomic, Molecular and Optical Physics
J. Phys. B: At. Mol. Opt. Phys. **50** (2017) 235604 (11pp) https://doi.org/10.1088/1361-6455/aa8c9f

Attosecond polarization control in atomic RABBITT-like experiments assisted by a circularly polarized laser

D I R Boll[1] **and O A Fojón**[1,2]

[1] Instituto de Física Rosario, CONICET-UNR, Blvd. 27 de Febrero 210 bis, 2000 Rosario, Argentina
[2] Escuela de Ciencias Exactas y Naturales, FCEIA, Universidad Nacional de Rosario, Argentina

E-mail: boll@ifir-conicet.gov.ar

Received 11 April 2017, revised 25 August 2017
Accepted for publication 14 September 2017
Published 31 October 2017

Abstract

We study theoretically the single ionization of noble gas atoms by the combined action of an attosecond pulse train with linear polarization and an assistant laser field with circular polarization. We employ a non-perturbative model that under certain approximations gives closed-form expressions for the angular distributions of photoelectrons. Interestingly, our model allow us to interpret these angular distributions as two-centre interferences where the orientation and the modulus of the separation vector between the virtual emitters is governed by the assistant laser field. Additionally, we show that such a configuration of light fields is similar to the polarization control technique, where both the attosecond pulse train and the assistant laser field have linear polarizations whose relative orientation may be controlled. Moreover, in order to compare our results with the available experimental data, we obtain analytical expressions for the cross sections integrated over the photoelectron emission angles. By means of these expressions, we define the 'magic time' as the delay for which the total cross sections for atomic targets exhibit the same functional form as the one of the monochromatic photoionization of diatomic molecular targets.

Keywords: atoms, photoionization, attopulses, laser

(Some figures may appear in colour only in the online journal)

1. Introduction

Attosecond radiation in the form of isolated pulses and trains of pulses were obtained in 2001 and became the cornerstone of the still-growing branch of science called attophysics. These (trains of) pulses are routinely produced by a high-order harmonic generation (HHG) process by focusing an intense ultrashort infrared laser field pulse into a noble gas atom chamber [1]. Due to the low intensity of the attosecond pulses obtained in this way, the most fruitful scheme is achieved by combining the attosecond pulse (train) with a remanent part of the generating laser, resembling the traditional pump-and-probe arrangement in time-resolved spectroscopy.

In particular, the combination of an attosecond pulse train (APT) with a low intensity near-infrared (NIR) laser field gives rise to the so-called reconstruction of attosecond beating by interference of two-photon transition (RABBITT) technique [2]. Although it is possible to obtain attosecond pulse trains with different properties [3, 4], the simplest ones have a discrete frequency spectrum containing only the odd harmonics of a given fundamental frequency. Therefore, the photoelectron spectrum for a RABBITT scheme implemented with these attosecond pulse trains, presents dressed harmonic lines populated (mainly) by the single-photon ionization of the target by the APT. Between consecutive dressed harmonic lines, the spectra presents sideband lines populated mainly by wavepackets that exchange an additional NIR photon. As a consequence, the sideband population is produced by wavepackets that follow different quantum paths and the interference between them may be controlled changing the delay between the APT and the NIR (henceforth delay).

Alternatively, an isolated attosecond pulse in combination with a stronger NIR leads to the attosecond streak camera [5, 6]. The ionization of an atomic or molecular target with a single attosecond pulse produces a photoelectron wavepacket in the continuum that interacts with the assistant laser field. This interaction produces a shift in the photoelectron energy according to the instantaneous value of the NIR vector potential at the time of the wavepacket injection into the continuum [5]. In this way, the instantaneous value of the assistant laser field vector potential may be traced from the photoelectron spectrum considered as a function of the delay [7].

More recently, angular streaking was demonstrated [8]. In this scheme, only a strong femtosecond laser field with a nearly circular polarization is employed. The highly nonlinear ionization probability for this reaction increases in the small windows of time near the extrema of the electric field, and thus the ionization instant is mapped to the final angle of the momentum vector in the polarization plane [8]. Consequently, this scheme is able to produce measurements with attosecond precision employing only femtosecond lasers.

Another extensively employed configuration is that of polarization control [9–11]. In this scheme, the vast majority of experiments are performed with linearly polarized monochromatic ionizing radiation, assisted by a low intensity NIR laser field with linear polarization along a tunable direction. Using this configuration for different relative orientations of the fields it is possible, for instance, to measure the relative partial wave contributions for a photoelectron in the continuum [9].

To the best of our knowledge, only one exception to the rule of monochromatic ionizing radiation for the polarization control technique is encountered in the literature [12], whereas the low NIR intensity condition persists even in these experiments. On the theoretical side, the reason for this may be traced to the inherently difficult task of taking into account the contributions from several harmonics and their mutual interferences [9]. As a consequence of the multiphoton transitions, an appropriate description of the reaction requires theoretical treatment beyond the second-order perturbation, which is not simple at all.

Solving the time-dependent Schrödinger equation for reactions such as the photoionization of multielectronic atomic targets assisted by an NIR laser field represents a challenge for current computational resources [13]. The use of simplified models leading to predictions in reasonable agreement with *ab initio* calculations and/or experimental results reveals as a valuable option to understand the physical processes involved, as the numerical results do not often have a straightforward interpretation.

Nowadays, several models able to describe reactions assisted by stronger NIR laser fields are available. Among them, the soft-photon approximation [14] was successfully applied to study angular distributions in laser-assisted atomic photoionization by photons from a free-electron laser [9] or high harmonic generation [13, 15] sources. Moreover, the separable Coulomb–Volkov (SCV) model was revealed as a versatile alternative to provide in certain situations quite accurate results or at least in qualitative agreement with *ab initio* calculations for atomic or molecular targets [16–18].

More recently, and based on an extension of the SCV model [19], we obtained non-perturbative closed-form expressions for the angular distribution of photoelectrons ionized by attosecond pulse trains in the presence of an NIR laser field. These expressions are similar to the ones corresponding to the monochromatic photoionization of diatomic molecular targets aligned in the direction of the NIR polarization, with a separation between virtual emitters that depends on the amplitude and frequency of the NIR electric field and the delay. An excellent agreement between our analytical results and the experimental angular distributions for atomic targets [15, 20] was found.

In this paper, we extend our study of the laser-assisted photoionization of atomic targets to the case of assistant laser fields with circular polarization. Moreover, we show that if the fast stage (photoionization) of the reaction is performed by an attosecond pulse train of in-phase odd harmonics, the result is analogous to the polarization control technique for an assistant laser field with linear polarization along a tunable direction. Alternatively, the results may be considered as a crossover between the RABBITT and angular streaking schemes, where the delay, and thus the instantaneous NIR electric field direction, is mapped into an specific orientation of the virtual emitters. Closed-form expressions for angle-integrated and angle-resolved cross sections of sidebands and dressed harmonics lines are provided.

Atomic units are used throughout otherwise explicitly stated.

2. Theory

Let us consider the photoionization of atomic targets by a train of attopulses arising from HHG assisted by a circularly polarized monochromatic laser in the NIR region. Let us assume that the intensity of each harmonic in the train is sufficiently low, so they may ionize the target only through single-photon processes [2]. Considering the single-active-electron approximation, the interaction of the electron in the atom with the train of attopulses (the first stage of the SCV approach) may be treated in the frame of the time-dependent perturbation theory [13, 21]. On the other hand, the assistant laser field may easily induce multiphoton transitions in the continuum (the third stage of the SCV approach) requiring a non-perturbative treatment. Therefore, the transition matrix amplitude within the dipole approximation in the velocity gauge is given by

$$M_{\mathrm{SCV}}(\mathbf{p}) = -\mathrm{i}\int_{-\infty}^{\infty} \mathrm{d}t\ \langle \Psi_f(\mathbf{r}, t)|\mathbf{A}(t)\cdot\hat{\mathbf{p}}|\Psi_i(\mathbf{r}, t)\rangle, \qquad (1)$$

where $\mathbf{p}$ is the photoelectron momentum associated to the momentum operator $\hat{\mathbf{p}}$ and $\Psi_{i,f}(\mathbf{r}, t)$ are the wavefunctions in the initial and final channels of the reaction, respectively. The vector potential $\mathbf{A}(t)$ represents the attosecond pulse train and it can be expressed as a combination of harmonics with a

Gaussian envelope,

$$\mathbf{A}(t) = \mathbf{\Pi} \sum_j A_j \mathrm{e}^{-\mathrm{i}j\omega_0 t} \mathrm{e}^{\mathrm{i}\phi_j} \mathrm{e}^{-t^2/2\tau_\mathrm{T}^2}, \tag{2}$$

where $\mathbf{\Pi}$ is the polarization vector, ω_0 is the fundamental frequency and ϕ_j is the individual phase of each frequency component whose amplitude is given by A_j, respectively. The full-width at half-maximum (FWHM) duration of the train is related to the parameter τ_T through the expression $\tau_\mathrm{FWHM} = 2\sqrt{2\ln 2}\,\tau_\mathrm{T}$.

The effect of the assistant laser field on the initially bound atomic states has been considered previously [21–24]. It was shown that bound–continuum transitions from atomic states with large ionization and excitation energies are barely affected when the laser field intensity is small or moderate, and the photoelectron energy is sufficiently far from the ionization threshold. Therefore, we neglect the polarization and the ionization due to the assistant laser field. Under this approximation, the state of the system in the initial channel of the reaction may be described by the laser-free wavefunction,

$$\Psi_i(\mathbf{r}, t) \approx \psi_i^0(\mathbf{r}) \mathrm{e}^{\mathrm{i}I_p t}, \tag{3}$$

where I_p is the ionization potential associated with the initial atomic orbital $\psi_i^0(\mathbf{r})$.

The final channel of the reaction, where the interaction between the photoelectron and the assistant laser field is treated to all orders, is represented through the ansatz [16, 18, 19],

$$\Psi_f(\mathbf{r}, t) \approx \psi_f^0(\mathbf{r}) \exp\left\{-\frac{\mathrm{i}}{2}\int^t [\mathbf{p} + \mathbf{A}_L(t')]^2 \mathrm{d}t'\right\}, \tag{4}$$

where $\psi_f^0(\mathbf{r})$ is the laser-free continuum wavefunction with asymptotic momentum $\mathbf{p}$. The importance of including the Coulomb interaction between the released photoelectron and the parent ion, particularly for photoelectrons with relatively low kinetic energy, was highlighted in previous works [21, 23]. A widespread theoretical approach leading to analytic results is to account for this interaction through the use of the wavefunction

$$\psi_f^0(\mathbf{r}) = (2\pi)^{-3/2} \mathrm{e}^{\mathrm{i}\mathbf{p}\cdot\mathbf{r}} N_p G(\mathbf{r}), \tag{5}$$

that represents asymptotically the Coulomb interaction of the residual target with the photoelectron, where $N_p = \mathrm{e}^{\pi\nu/2}\Gamma(1 + \mathrm{i}\nu)$, $\nu = Z_f/p$ being Z_f the net charge of the residual target and $G(\mathbf{r}) = {}_1F_1(-\mathrm{i}\nu;\, 1;\, -\mathrm{i}(pr + \mathbf{p}\cdot\mathbf{r}))$ is the confluent hypergeometric function.

In contrast with our previous work [19], where a linearly polarized assistant laser field was considered, in this case we take into account a circularly polarized assistant laser field with vector potential $\mathbf{A}_L(t)$ given by,

$$\mathbf{A}_L(t) \simeq -\frac{\mathbf{E}_z}{\omega_0}\sin(\omega_0 t - \phi_L) - \frac{\mathbf{E}_y}{\omega_0}\cos(\omega_0 t - \phi_L), \tag{6}$$

and, consequently,

$$\mathbf{E}_L(t) = -\frac{\partial \mathbf{A}_L(t)}{\partial t} \tag{7}$$

$$\simeq \mathbf{E}_z \cos(\omega_0 t - \phi_L) - \mathbf{E}_y \sin(\omega_0 t - \phi_L) \tag{8}$$

where $|\mathbf{E}_z| = |\mathbf{E}_y|$ are the amplitudes of the electric field along the Cartesian axes z and y in the laboratory frame, respectively, and ϕ_L is a phase related to the delay t_0 through the relation $\phi_L = \omega_0 t_0$.

As we noted previously [19], the transition matrix amplitudes in equation (1) for an atomic target with initial and final states described by equations (3) and (4), respectively, photo-ionized by an in-phase odd-harmonics APT assisted by an NIR laser, are given by,

$$M_\mathrm{SCV}(\mathbf{p}_q) \propto M_{ph}(\mathbf{p}_q)(\mathrm{e}^{\mathrm{i}\mathbf{p}_q\cdot\boldsymbol{\alpha}_0} \pm \mathrm{e}^{-\mathrm{i}\mathbf{p}_q\cdot\boldsymbol{\alpha}_0}), \tag{9}$$

when the asymptotic photoelectron momentum satisfies the relation $p_q^2/2 + I_p + U_p = q\omega_0$, being $U_p = |\mathbf{E}_z|^2/2\omega_0^2$ the ponderomotive energy. The plus sign applies to the case of dressed harmonic (DH) lines, described by an odd integer number q. On the other hand, the minus sign applies to the case of sideband (SB) lines, described by an even integer number q. The monochromatic transition matrix amplitude $M_{ph}(\mathbf{p}_q)$ is given by,

$$M_{ph}(\mathbf{p}_q) = -\mathrm{i}\langle\psi_f^0(\mathbf{r})|\mathbf{\Pi}\cdot\nabla_r|\psi_i^0(\mathbf{r})\rangle, \tag{10}$$

and the vector $\boldsymbol{\alpha}_0$ corresponds to the classical excursion of a free electron in the presence of the electric field $\mathbf{E}_L(t)$, evaluated at time $t = 0$. Considering the vector potential $\mathbf{A}_L(t)$ in equation (6), we get for the classical excursion vector,

$$\boldsymbol{\alpha}(t) = \int^t \mathbf{A}_L(t')\mathrm{d}t' \tag{11}$$

$$= \frac{\mathbf{E}_z}{\omega_0^2}\cos(\omega_0 t - \phi_L) - \frac{\mathbf{E}_y}{\omega_0^2}\sin(\omega_0 t - \phi_L), \tag{12}$$

that evaluated at time $t = 0$ yields,

$$\boldsymbol{\alpha}(0) = \boldsymbol{\alpha}_0 = \frac{\mathbf{E}_z}{\omega_0^2}\cos\phi_L + \frac{\mathbf{E}_y}{\omega_0^2}\sin\phi_L, \tag{13}$$

indicating that the orientation of the vector $\boldsymbol{\alpha}_0$ depends on the delay ϕ_L. As according to equation (9) the virtual emitters are located at $\pm\boldsymbol{\alpha}_0$, we may define the separation vector as $\mathbf{R}_L = 2\boldsymbol{\alpha}_0$ to finally get the following expressions for the differential cross section of SB and DH lines,

$$\frac{\mathrm{d}\sigma}{\mathrm{d}\Omega_e}(\mathbf{p}_q) \propto |M_{ph}(\mathbf{p}_q)|^2 \sin^2(\mathbf{p}_q\cdot\mathbf{R}_L/2) \quad \text{(SBs)} \tag{14}$$

$$\frac{\mathrm{d}\sigma}{\mathrm{d}\Omega_e}(\mathbf{p}_q) \propto |M_{ph}(\mathbf{p}_q)|^2 \cos^2(\mathbf{p}_q\cdot\mathbf{R}_L/2) \quad \text{(DHs)} \tag{15}$$

respectively, where $\mathrm{d}\Omega_e = \sin\theta_e \mathrm{d}\theta_e \mathrm{d}\phi_e$ is the differential solid angle element in the photoelectron emission direction as measured from the polarization vector $\mathbf{\Pi}$. Detailed analyses of the physical interpretation of the vector $\mathbf{R}_L$ as well as the expected behaviour in the low NIR intensity limit of the above expressions can be found in [19].

We point out here that the differential cross sections for the ionization of an atom by a sequence of in-phase odd harmonics in the presence of a circularly polarized NIR are analogous to those of the monochromatic ionization of a homonuclear diatomic molecule with internuclear separation $\mathbf{R}_L$ [25–28], whose orientation is given by the instantaneous NIR electric field direction at time $t = 0$. In this analogy (see

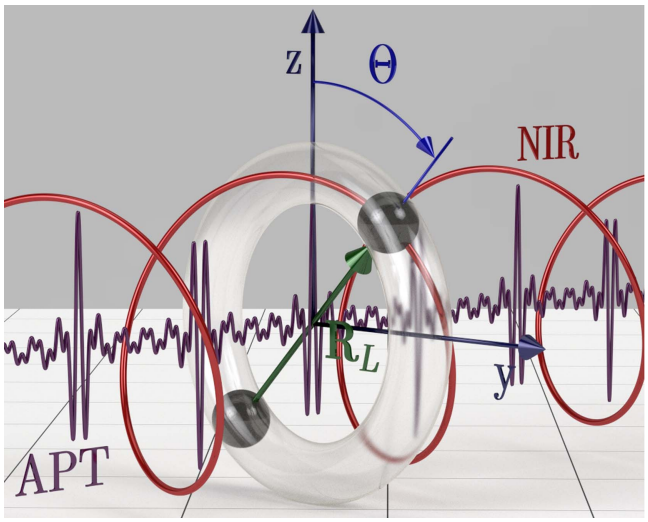

Figure 1. Pictorial representation of the reaction. A linearly polarized APT photoionizes an atomic target in the presence of a circularly polarized assistant laser field. The photoelectron angular distribution for the reaction is modulated by the interference of signals arising from two virtual emitters (dark grey spheres). The polar angle Θ is related to the delay ϕ_L through the relation $\tan\Theta = \tan\phi_L$.

a pictorial representation in figure 1), the DHs (SBs) play the role of the bound–continuum transition of molecules from an initial state of *gerade* (*ungerade*) symmetry.

In addition, the equations (14) and (15) bear some resemblance with the ones describing some interference effects in the recombination step of the HHG process in aligned molecular targets [29–31]. In turn, the suppression of the harmonic emission observed in that process, for some photon energies, was attributed to this interference mechanism [31–33]. In the latter, the crucial parameters to describe the phenomenon are the molecular orientation and the de Broglie wavelength of the photoelectron ($\lambda_q = 2\pi/p_q$). Therefore, this allow us to identify some parallelisms between our results for atomic targets with those for the HHG in aligned molecular targets.

In our previous work on linearly polarized assistant laser fields [19], we showed that a change in the delay results in different values for the modulus of $\mathbf{R}_L$. In contrast, for the circularly polarized assistant laser field considered here a change in the delay ϕ_L gives place to different orientations of the vector $\mathbf{R}_L$, whereas its modulus is preserved.

In figure 1, we show a pictorial representation of the reaction corresponding to the ionization of an atomic target by an attosecond pulse train assisted by a circularly polarized laser field. The single-photon ionization of the target is induced by the APT with in-phase odd harmonics linearly polarized along the z axis in the laboratory frame. Due to the APT temporal structure, containing two opposite pulses per NIR cycle, the reaction is characterized by the interference of the signals emerging from two virtual emitters located at $\pm\boldsymbol{\alpha}_0$. Moreover, as indicated in equation (13), the position of the virtual emitters is related to the NIR electric field properties and, therefore, different orientations of the virtual dimer may be obtained changing the delay ϕ_L. Finally, as the instantaneous assistant laser field vector at the ionization times points to the specific directions $\pm\boldsymbol{\alpha}_0$, this behaviour is reminiscent to the polarization control [9, 12] and/or the angular streaking [8], or even the HHG process for oriented molecular targets [31, 32].

To calculate the photoionization differential cross sections (or alternatively, the angular distributions) for atomic targets by using equations (14) and (15), we need to compute the square modulus of the monochromatic photoionization amplitude $M_{ph}(\mathbf{p}_q)$. Now, provided that the magnetic sublevels of the atomic target are equally populated, the differential cross sections for the photoionization by linearly polarized monochromatic radiation has the general form [34],

$$\frac{\mathrm{d}\sigma^{(at)}}{\mathrm{d}\Omega_e}(\mathbf{p}_q) = \frac{\sigma_{\mathrm{tot}}}{4\pi}[1 + \beta P_2(\cos\theta_e)] \propto |M_{ph}(\mathbf{p}_q)|^2, \quad (16)$$

where σ_{tot} is the total photoionization cross section, β is the asymmetry parameter, and $P_2(x) = (3x^2 - 1)/2$ is the second-order Legendre polynomial.

The measurement of angularly resolved cross sections for these reactions is not simple at all and, usually, the available experimental data are given in the angle-integrated form. Therefore, analytical expressions for the total cross sections for these reactions may be useful for the interpretation of the photoelectron spectra. Keeping this in mind, we present in the following the results for the cross sections integrated over the photoelectron emission angles, corresponding to SB and DH lines. From equations (14), (15) and (16), the angle-integrated cross sections for SB and DH lines are given by,

$$\sigma(p_q) \propto \frac{\sigma_{\mathrm{tot}}}{4\pi}\int \mathrm{d}\Omega_e[1 + \beta P_2(\cos\theta_e)]\begin{cases}\sin^2(\mathbf{p}_q \cdot \mathbf{R}_L/2)\\ \cos^2(\mathbf{p}_q \cdot \mathbf{R}_L/2)\end{cases} \quad (17)$$

After integration, the total cross sections reads (see appendix),

$$\sigma(p_q) \propto \frac{\sigma_{\mathrm{tot}}}{2}[1 \mp j_0(p_q R_L) \pm \beta j_2(p_q R_L) P_2(\cos\Theta)], \quad (18)$$

where Θ is the polar angle defining the direction of the vector $\mathbf{R}_L$ in the laboratory frame and $j_n(z)$ is the spherical Bessel function of order n. As before, taking account the definition $\mathbf{R}_L = 2\boldsymbol{\alpha}_0$, equation (13) provides the link between the direction of the vector $\mathbf{R}_L$ and the delay through $\tan\Theta = \tan\phi_L$. Thus, the total photoionization cross sections depend on the delay through the variable Θ, on the laser intensity through the modulus R_L and on the asymptotic photoelectron momentum modulus p_q.

In addition, an interesting result may be obtained from equation (18). Supposing that $p_q \sim p_{q+1}$, the sum $\sigma(p_q) + \sigma(p_{q+1})$ gives the total cross section σ_{tot} corresponding to the monochromatic photoionization of the target. This analytical expression accounts for the population transfer between sidebands and dressed harmonic lines previously observed in theoretical [35] and experimental [9] results. Moreover, this population transfer expresses the fact that the assistant laser field does not contribute to the primary photoionization process [9]. In this case, the role of the assistant

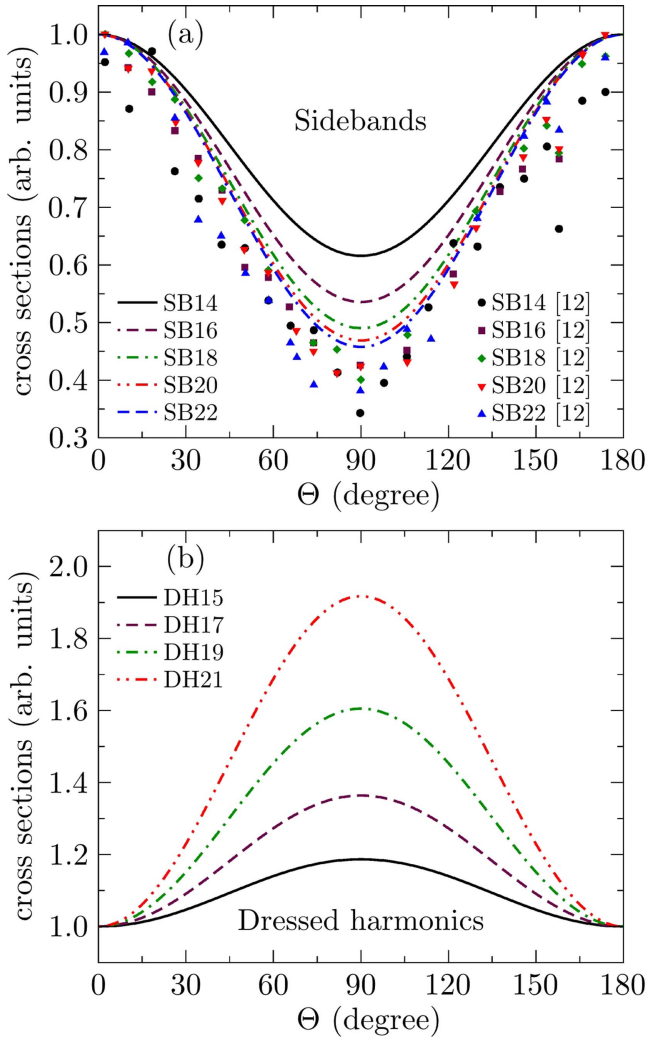

Figure 2. (a) Angle-integrated (total) cross sections of several sideband lines as a function of the relative angle Θ, for atomic Ar targets. The different lines indicate our results obtained by means of equation (18) and the different symbols the experimental results from [12]. (b) Same as (a) but for the dressed harmonic lines.

laser field is limited to merely redistribute the probabilities among the accessible final states.

3. Results and discussion

We present in figure 2 our results for the total cross sections of several SB and DH lines, corresponding to the photoionization of an atomic Ar target by an in-phase odd-harmonics APT, assisted by a circularly polarized NIR laser with a wavelength of 810 nm. These results are obtained from equation (18) for an NIR laser intensity of $I_L = 1 \times 10^{12}$ W cm^{-2}, and the corresponding β values are interpolated from theoretical data [36]. Additionally, we show in figure 2(a) the available experimental results for the polarization control scheme, obtained for different relative orientations between the APT and a linearly polarized assistant laser field [12].

In this case, we observe satisfactory agreement between our analytical results and the experiments for the higher-order sidebands. In contrast, the experimental results for the lowest order sidebands (SB14, SB16) are overestimated by our model, although a qualitative description is obtained. The reasons for these quantitative discrepancies are not clear. Firstly, as the experimental results show the same functional behaviour for all the sidebands, the influence of the resonant $3s - np$ excitations may be neglected [12]. Moreover, the discrepancies cannot be explained by the presence of higher-order transitions in the continuum, because they are included to all order in our model. Instead, its origin may be related to effects not taken into account, or even an inaccuracy of the model for low photoelectron energies. However, our model was proved to be correct in a more stringent test such as the photoelectron angular distributions for the same atomic target with similar photoelectron energies and laser field intensities [19]. Therefore, it is not clear why the integrated cross sections are not well reproduced.

One could argue that deviations come from the fact that we are employing harmonics with constant phase and amplitudes. However, we have checked that a restricted model considering continuum–continuum transitions up to one NIR photon [19] with amplitudes and phases of each neighbour harmonic taken as a free-fitting parameter is also unable to improve the description. The reason behind this behaviour may be traced to the inherent spatial and temporal separation in the SCV model [16, 18]. As a consequence, the amplitude and phase of each neighbour harmonic to a given sideband can be factored from the squared modulus of the transition matrix amplitudes, in the second-order perturbative limit of our model [37]. In turn, this leads to sidebands independent of these quantities when they are normalized.

Additionally, the predictions of our analytical non-perturbative model are in very good agreement with previously reported theoretical results [12] that, for the sake of clarity, are not shown here. Moreover, we have checked that the differences between our theoretical results and those from [12] are smaller than approximately 4% (or 12%, depending on the set of β values considered) for every sideband index q. This result is not coincidental. As a matter of fact, by taking a series expansion of each spherical Bessel function in our result of equation (18) and retaining terms up to the second order, the normalized total cross sections for SB lines read,

$$\sigma_{\mathrm{SB}} \propto \left(1 - \frac{3\beta \sin^2 \Theta}{5 + 2\beta}\right), \tag{19}$$

a result that is exactly the same as the one obtained in [12] for the normalized SB signals in the polarization control scheme. Moreover, our result is valid independently of the symmetry of the initial state as in [11].

The small discrepancies between both theoretical results may be understood by recalling that the characteristic number of NIR photons exchanged by the photoelectron and the assistant laser field may be estimated from $N_{\mathrm{eff}} \sim p|\mathbf{E}_L|/\omega_0^2$ [37, 38]. Therefore, as $N_{\mathrm{eff}} \sim 1$ for the present conditions, the perturbative expansion in equation (19) represents a good approximation to our full-order results for the cross sections

integrated over the photoelectron emission angles, as shown in equation (18).

On the other hand, figure 2(b) shows the results for the dressed harmonics lines, where the opposite trend is observed since the signal for each line grows with the index q. This may be related to the population transfer between sidebands and dressed harmonic lines mentioned at the end of the previous section. As before, the assistant laser field does not contribute to the primary photoionization process so any change in the SB (DH) lines is (approximately) compensated with an opposite variation in the DH (SB) lines.

Additionally, equation (18) may be recast into a more usual form,

$$\sigma_{\mathrm{SB,DH}} \propto [1 + \beta_{\mathrm{SB,DH}} P_2(\cos\Theta)], \tag{20}$$

with a modified asymmetry parameter given by,

$$\beta_{\mathrm{SB,DH}} = \pm \frac{\beta j_2(p_q R_L)}{1 \mp j_0(p_q R_L)}, \tag{21}$$

where the upper (lower) sign corresponds to the SB (DH) lines case. Consequently, the total cross section for SB and DH lines as a function of the delay, for a given assistant laser field, behaves as the differential cross section for the monochromatic photoionization by linearly polarized radiation with a modified asymmetry parameter, and where the polar angle Θ in the former plays the role of the photoelectron emission direction in the later. Moreover, this analogy also applies to the molecular case, where the angular distribution of photoelectrons emitted from randomly oriented molecular targets follows the same functional behaviour [39]. Again, the polar angle Θ plays the role of the photoelectron emission angle. Generally, these results are a consequence of conservation of parity and angular momentum [39–41]. We will return to this point later when we discuss the angle-resolved cross sections.

Moreover, as the modified asymmetry parameters defined in equation (21) depend on the asymptotic photoelectron momentum p_q and the assistant laser field intensity through the variable R_L, we study their dependence with the product $p_q R_L$. The results corresponding to the modified asymmetry parameters as a function of $p_q R_L$ obtained with equation (21) are shown in figure 3 by the full lines. Additionally, we show the results for the first term in a Taylor series expansion of equation (21).

As can be seen, for DH lines, the first term in the Taylor series expansion for the modified asymmetry parameter is nearly identical to the full results in the range of $p_q R_L$ values considered previously (grey-shaded area). This behaviour is consistent with the physical picture of undisturbed DH lines by the presence of neighbour harmonics in the low NIR laser intensity limit. In contrast, for SB lines, including the continuum–continuum transitions to all order leads to a smaller modified asymmetry parameter as compared with the one given by the first term in the Taylor series expansion of equation (21). This, in turn, qualitatively explains the small differences encountered when comparing the results for the total cross sections of sideband lines obtained by means of equations (18) and (19).

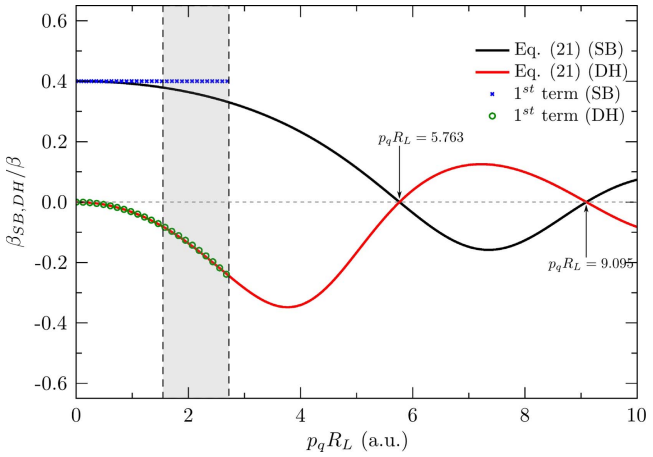

Figure 3. Modified asymmetry parameters for SB and DH lines as a function of $p_q R_L$, as given by equation (21) (full lines). The crosses and circles correspond to the first term in a Taylor series expansion of equation (21) for SB and DH lines, respectively. The grey-shaded region indicates the range of values $p_q R_L$ corresponding to the figure 2, and the arrows show the values for which the modified β for SH and DH lines are zero.

In addition, the transformed asymmetry parameters given by equation (21) remain inside the same limits for the usual β parameter, i.e., $-1 \leqslant \beta \leqslant 2$ [34]. Just a visual inspection of figure 3 is sufficient to conclude that $\beta_{\mathrm{SB,DH}} \in (-0.7, 0.8]$, for every possible β value. This feature of the modified asymmetry parameter prevents the observation of zeros for the total cross sections induced by the assistant laser field. However, an appropriate choice of the parameters p_q , R_L and Θ may lead to the obtention of cross sections several times smaller than the total atomic cross section in the monochromatic case for the same photoelectron kinetic energy.

In addition, the crossing of the curves for β_{SB} and β_{DH} occurs at the zeros of $j_2(z)$ predicting a cross section for SB and DH lines independent of the relative polarization angle Θ. This, in turn, indicates that the dependence of the total cross section with the delay is lost for these values of $p_q R_L$. Of course, these values of the product $p_q R_L$ may require exceedingly high intensities of the assistant laser field for small values of the asymptotic momentum p_q, leading to a possible breakup of our model. However, for photoelectrons with high enough kinetic energy, the laser field intensity required to achieve this behaviour fulfils the validity conditions of our model.

Furthermore, for every value of the product $p_q R_L$ if the delay is equal to $\phi_L \sim 54.7°$ then, as $\Theta = \phi_L$ the equation (18) reduces to $\sigma_{\mathrm{tot}}(1 \mp \sin(p_q R_L)/p_q R_L)$, i.e., the total photoionization cross sections of the atomic target multiplied by the Cohen–Fano interference factor [25]. So, we can call this delay as 'magic time' in analogy with the well-known magic angle for the monochromatic photoionization. Additionally, we point out here that a similar expression for the total photoionization cross sections for diatomic molecular targets may be obtained after integration over the molecular orientation and the photoelectron emission direction. In turn, as shown in [28, 42], such an expression may be used to

analyse the oscillatory behaviour associated with interferences due to the coherent emission in the total photoionization cross sections of diatomic molecular targets, particularly at high photoelectron energies. Therefore, for a delay equal to the magic time, the analytical results for the total cross sections for the laser-assisted photoionization of atomic targets obtained with our model reduce to the (asymptotic) total cross sections corresponding to a diatomic molecular target. An analogous situation is found when $\beta_{\mathrm{SB,DH}} = 0$, but in this case the result is independent of the delay.

As previously noted for the molecular photoionization case [39, 43], much clearer evidence of the interference mechanisms may be obtained from the fully differential cross sections. Moreover, in a previous paper [19] we found the conditions for the obtention of totally constructive or destructive interferences for SB and DH lines in the laser-assisted photoionization of atomic targets by a train of attosecond pulses. In the latter, we consider that both the attosecond pulse train and the assistant laser field are linearly polarized. Therefore, a variation of the delay ϕ_L translates into different values of R_L. In contrast, for the circularly polarized assistant laser field considered here, a modification of the delay implies a different orientation of $\mathbf{R}_L$ while its modulus is preserved. Moreover, from the above analysis, it is expected that RABBITT-like reactions employing an assistant laser field with arbitrary elliptical polarization behave as a mix of the linear and circular cases.

In order to gain a deeper insight on the effects induced by the totally constructive and destructive interferences for the reaction of interest, we calculate the angle–delay spectra for atomic Ar targets and two different NIR intensities by means of equations (14) and (15). Additionally, as the equation (13) indicates that the delay ϕ_L is mapped identically to a definite orientation of the vector $\mathbf{R}_L = 2\boldsymbol{\alpha}_0$, these spectra may be associated with angle–angle spectra. One of these angles (θ_e) corresponds to the electron emission polar angle and the other (Θ) to the relative angle between the polarization direction of the APT and the vector $\mathbf{R}_L$ indicated in figure 1. These spectra, corresponding to emissions into the plane yz ($\phi_e = \pi/2$) in the laboratory frame, are shown in figure 4.

It can be seen that the spectra for the SB18 remain almost unchanged when the NIR intensity is increased, except in the middle part where minor differences are observed. This finding may be related to the fact that sidebands are less sensitive to variations in the laser intensity, as shown previously for the case of an assistant laser field with linear polarization [19]. The condition for obtaining totally destructive interferences in sideband lines for an emission at angles other than $\mathbf{p}_q \perp \mathbf{R}_L$ requires twice the photoelectron momentum (or, alternatively, twice the electric field amplitude) compared to the dressed harmonic lines case. As expected, the totally destructive interferences for emission in a direction perpendicular to $\mathbf{R}_L$, indicated by the dashed lines in figures 4(a) and (b), are obtained, irrespective of the laser intensity.

In contrast, the spectra for the dressed harmonic line DH19 in figures 4(c) and (d) show profound modifications when the assistant laser field intensity is increased. This is in agreement with the linear polarization case [15, 19, 20] where the angular distributions corresponding to these spectral lines evolve notably even for small changes in R_L. For the lower intensity case in figure 4(c), two lobes may be identified corresponding to the totally constructive interference for electron emission in the direction perpendicular to $\mathbf{R}_L$. This constructive interference mechanism is preserved regardless of the assistant laser field intensity. In contrast, for the higher intensity case in figure 4(d), the product $\mathbf{p}_q \cdot \mathbf{R}_L/2$ satisfies (for certain emission angles) the condition for the obtention of totally destructive interferences. This interference pattern is highlighted in figure 4(d) by the dashed oblique lines that indicate a forbidden photoelectron emission for those conditions.

To analyse further these angle-resolved photoelectron spectra, we calculate the three-dimensional photoelectron angular distributions (PADs) for both laser intensities and some representative delays (different Θ values). The results are shown in figure 5 and, in general, it can be seen that changing the delay in a quarter of the period ($T_L = 2\pi/\omega_0 \sim 2.7$ fs) of the assistant laser field induces strong variations in the PADs allowing thus the sub-femtosecond control of the photoelectron angular distributions.

Let us begin the analysis of these angular distributions by studying the results for the sideband SB18. According to equation (14), the PADs for these spectral lines present a nodal plane perpendicular to $\mathbf{R}_L$ irrespective of the NIR intensity. The presence of such nodal planes is more evident for the delays $\Theta = 0$, $\pi/2$ where xy and xz, respectively, are the corresponding planes in the laboratory frame.

In particular, the PADs for $\Theta = 0$ show a pseudo-p character which is qualitatively consistent with the results expected from the dipole selection rules: starting from an initial orbital with p symmetry and considering that the sidebands are populated by transitions involving the exchange of an even number of photons (one APT photon plus an odd number of NIR photons), only wavepackets associated to an odd angular momentum value may be populated.

Alternatively, to understand these results it is helpful to expand the angular distributions in spherical harmonics. As usual for diatomic molecular targets [39], the expansion is done in the molecular frame where the quantization axis is given by the internuclear separation vector. In our case, this role is played by the vector $\mathbf{R}_L$. After lengthy but otherwise straightforward calculations that we omit here for the sake of brevity, we get,

$$\frac{\mathrm{d}\sigma}{\mathrm{d}\Omega}(\mathbf{p}_q) \propto \sum_{L=0}^{\mathrm{even}} \sum_{M=-2}^{2} A_{L,M} Y_{L,M}(\theta', \phi') \tag{22}$$

where θ' and ϕ' are the polar and azimuthal angles, respectively, that define the photoelectron emission direction in the molecular reference frame. Interestingly, for the differential cross sections given by the equations (14) and (15), the coefficients $A_{L,M}$ can be obtained in closed form. The expression shown in equation (22) is in full agreement with previous theoretical results for the resonant multiphoton

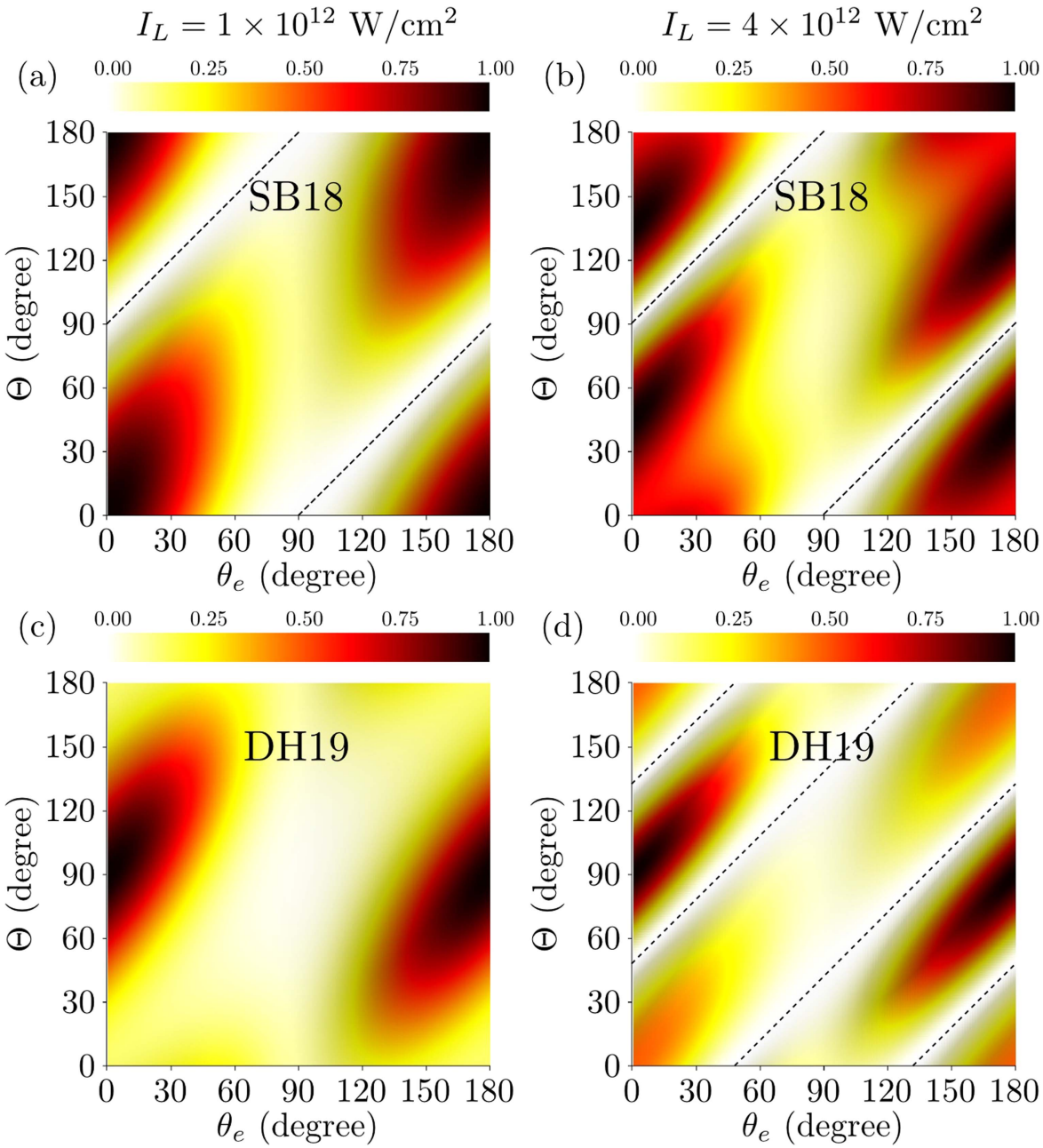

Figure 4. Angle–delay (Θ) spectra for the SB18 and the DH19 spectral lines corresponding to the photoionization of atomic Ar targets by a linearly polarized attosecond pulse train assisted by a laser field with circular polarization and different intensities. The dashed lines indicate the existence of totally destructive interferences.

ionization of isotropically distributed atomic or molecular targets in gas phase [41] and they result from the conservation of parity and angular momentum [40]. At variance with the results for the resonant multiphoton ionization, in our case the target is ionized after the absorption of only one APT photon and this property of the reaction is the responsible for the constraint $|M| \leqslant 2$.

It can be shown that for $\Theta = 0$ the expansion in equation (22) reduces to

$$\frac{\mathrm{d}\sigma}{\mathrm{d}\Omega}(\mathbf{p}_q) \propto \sum_{L=0}^{\text{even}} A_{L,0} Y_{L,0}(\theta', \phi'), \tag{23}$$

indicating that the pseudo-p character observed for the SB18 with $\Theta = 0$ is obtained combining spherical harmonics with the opposite parity which, in turn, satisfy the expected up-down symmetry in the molecular frame for these angular distributions. We want to stress here that these expansions in spherical harmonics usually show a quick convergence towards the results obtained with the full expressions. In turn, this means that a reasonable convergence is obtained after considering only a few values of L. For the lower intensity, the most important contribution comes from the term with $A_{2,0}$ closely followed by the one with coefficient $A_{0,0}$. For the

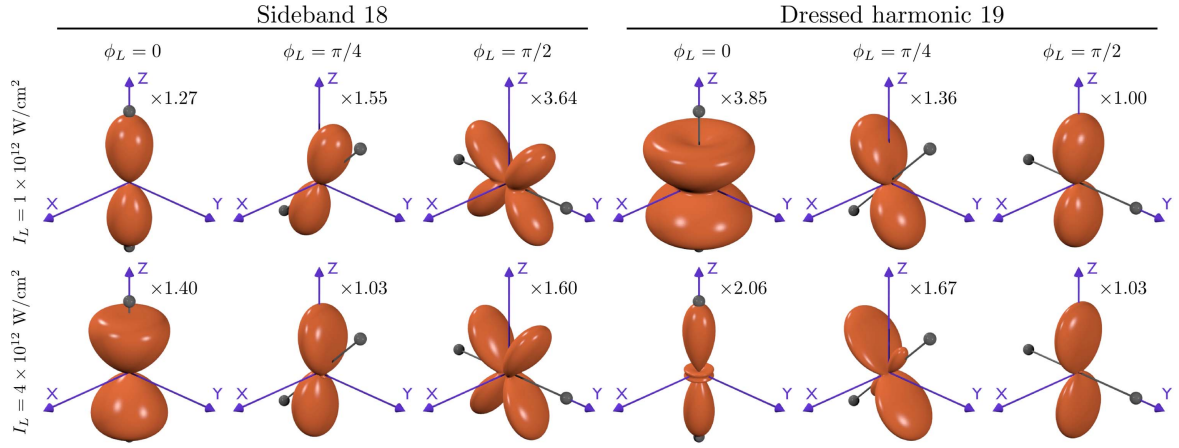

Figure 5. Three-dimensional photoelectron angular distributions in the SB18 and DH18 for some selected delays corresponding to $\Theta = 0, \pi/4, \pi/2$ and two different values of the assistant laser field intensity. The spatial orientation of the virtual emitters in indicated with two dark grey spheres. The indicated scaling factor for each PAD is calculated relative to the PAD for DH19, $\Theta = \pi/2$ and the lower intensity.

higher intensity, the ordering in importance of these coefficients is reversed.

In contrast, for $\Theta = \pi/4$ the symmetry of the system is broken and the full expression in equation (22) must be employed. However, a pseudo-p character may still be identified. Moreover, the skewing of the photoelectron angular distributions with respect to the vector $\mathbf{R}_L$ is a consequence of the contributions with $M = \pm 1$ [41]. An increase of the laser intensity implies larger contributions of these terms with a corresponding augmented skewing of the PADs, as can be seen upon comparison of the results for the lower and the higher NIR intensities.

The results for $\Theta = \pi/2$ are more interesting as they resemble the (real) spherical harmonic $Y_{2,-1}$, in apparent contradiction with the qualitative results expected from the dipole selection rules for sideband lines. Additionally, these results cannot be easily explained by means of equation (22), as the only restriction for the coefficients in this case is given by $A_{L,\pm 1} = 0$. In the lower intensity case, the properties observed in the PAD are a consequence of the nodal plane predicted by equation (14) that bisects the monochromatic angular distribution in the xz plane.On the other hand, for the higher intensity besides to the nodal plane perpendicular to $\mathbf{R}_L$, totally constructive interferences are predicted for emission angles $\theta' \sim 45°$ explaining the signal increase as compared with the lower intensity case.

Finally, the results for the dressed harmonic line DH19 show remarkable changes for the delay $\phi_L = 0$ when the intensity of the assistant laser field is modified. In this case, the strong modification of the probability of emission in the classical direction may be understood by means of the ratio between the de Broglie wavelength $\lambda_q = 2\pi/p_q$ associated to the photoelectron and the modulus of the vector $\mathbf{R}_L$. Whereas the wavelength for a photoelectron in the spectral line DH19 is $\lambda_q = 6.4$, the values for R_L corresponding to the lower and the higher intensities are 2.4 and 4.8, respectively. Consequently, for the lower intensity the interference factor in equation (15) is close to the totally destructive interference condition and explains the smaller photoelectron signal as compared to the PAD with the higher NIR intensity. For the delays $\phi_L = \pi/4, \pi/2$, the PADs are similar for both intensities, except for the larger skewing and the additional lobes nearly coincident with $\mathbf{R}_L$ in the case with $\phi_L = \pi/4$ and the larger NIR intensity. As in the sidebands case, the skewing may related to the contributions $A_{L,M}$ with $M = \pm 1$ in equation (22).

4. Conclusions

We generalize our recently developed non-perturbative model for the laser-assisted photoionization of atomic targets by attosecond pulse trains to the case of an assistant laser field with circular polarization. At variance with our previous results for an assistant laser field with linear polarization in [19] where the delay dependence is mapped to different separations of the virtual emitters predicted by the model, in this case the delay dependence is translated into different orientations of these virtual emitters whereas the distance between them is preserved. In addition to the expressions for the angle-resolved cross sections, we present analytical results for the angle-integrated ones. The latter are compared with the available experimental results for the polarization control technique, showing an overall good agreement with regards to the delay dependence particularly for the sidebands of higher order. Moreover, the results of our model show that the discrepancies between theoretical and experimental results for the sidebands of lower index are not related with continuum–continuum transitions of order higher than one.

Additionally, we show that the expressions for the angle-integrated cross sections may be recast into a well-known expression for the angular distribution of photoelectrons. In that case, the role of the polar emission angle is played by the polar angle defining the orientation of virtual emitters. In addition, we provide the expression for the modified asymmetry parameters corresponding to sidebands and dressed harmonic lines. The analysis of these modified asymmetry parameters allow us to conclude that, within the validity range of our model, the assistant laser field is not able to induce zeros in the total cross sections. However, an appropriate

selection of the system parameters gives place to a total cross section several times smaller than the monochromatic one and, more importantly, our results show that the total cross sections may be controlled just by changing the delay between the attosecond pulse train and the assistant laser field.

Moreover, we show that there exist a particular delay, that we call 'magic time', for which the total cross sections for the ionization of atomic targets by a train of attosecond pulses assisted by a circularly polarized laser field assume the same functional form corresponding to the total cross sections for the monochromatic photoionization of molecular targets given by Cohen–Fano.

Finally, we turn our attention to the angle-resolved cross sections. We find that the expansion of the angular distributions into a combination of spherical harmonics is in full agreement with previous results for the resonant multiphoton ionization of isotropically distributed targets. In addition, in our case, it is possible to obtain closed-form expressions for the coefficients in the expansion. These analytical results were employed to analyse the three-dimensional angular distributions obtained for different delays and intensities of the assistant laser field. Moreover, we show that by controlling the delay and the assistant laser field intensity it is possible to manipulate the photoelectron angular distributions by means of the interference mechanisms involved.

We expect that our results will be useful for promoting the research line of RABBITT-like experiments assisted by stronger infrared laser fields, by providing simple and yet accurate expressions for the observables of the reaction that account for the higher-order continuum–continuum transitions populating the different spectral lines when the intensity of the assistant laser field exceeds the limit imposed by the second-order approximations usually employed. Moreover, it is envisaged that employing chirped attosecond pulse trains and/or assistant laser fields with arbitrary elliptical polarization might lead to additional control mechanisms as observed previously for the high-order harmonic generation technique in molecular targets. Work in this direction is in progress.

Acknowledgments

Authors acknowledge financial support from the Agencia Nacional de Promoción Científica y Tecnológica (PICT No. 01912), the Consejo Nacional de Investigaciones Científicas y Técnicas de la República Argentina (PIP No. 11220090101026), and the Fundación Josefina Prats.

Appendix

In this appendix we provide an outline of the calculations performed to obtain the total cross sections as a function of the delay for SB and DH lines given in equation (18). These expressions are obtained integrating the equations (14) and (15) over the photoelectron emission angles, respectively, and are given by,

$$\sigma(p_q) \propto \frac{\sigma_{\rm tot}}{4\pi}\int \mathrm{d}\Omega_e[1+\beta P_2(\cos\theta_e)]\begin{cases}\sin^2(\mathbf{p}_q\cdot\mathbf{R}_L/2)\\ \cos^2(\mathbf{p}_q\cdot\mathbf{R}_L/2)\end{cases} \tag{A.1}$$

The scalar product $\mathbf{p}_q\cdot\mathbf{R}_L/2$ may be written as,

$$\frac{\mathbf{p}_q\cdot\mathbf{R}_L}{2} = \frac{p_q R_L}{2}[\sin\theta_e\sin\Theta\cos(\phi_e-\Phi)+\cos\theta_e\cos\Theta], \tag{A.2}$$

where the angles Θ and Φ define the orientation of $\mathbf{R}_L$ in the laboratory frame. Additionally, using the half-angle formulae to expand the squared trigonometric functions in equation (A.1) as $[1\mp\cos(\mathbf{p}_q\cdot\mathbf{R}_L)]/2$, respectively, it is possible to split the integral above as,

$$\sigma(p_q) \propto \frac{\sigma_{\rm tot}}{4\pi}[I_1+I_2+I_3+I_4+I_5+I_6], \tag{A.3}$$

where,

$$I_1 = \int \mathrm{d}\Omega_e\,\frac{1}{2} = 2\pi. \tag{A.4}$$

For the integral I_2 we obtain,

$$I_2 = \mp\frac{1}{2}\int_0^{\pi}\mathrm{d}\theta_e\sin\theta_e\cos(p_qR_L\cos\theta_e\cos\Theta) \times\int_0^{2\pi}\mathrm{d}\phi_e\cos(p_qR_L\sin\theta_e\sin\Theta\cos(\phi_e-\Phi)), \tag{A.5}$$

where the integral over ϕ_e can be obtained from [44]. The I_2 term results,

$$I_2 = \mp\pi\int_0^{\pi}\mathrm{d}\theta_e\sin\theta_e\cos(p_qR_L\cos\theta_e\cos\Theta) \times J_0(p_qR_L\sin\theta_e\sin\Theta), \tag{A.6}$$

which after the variable change $\xi=\cos\theta_e$, may be integrated as [44],

$$I_2 = \mp 2\pi\frac{\sin(p_qR_L)}{p_qR_L} = \mp 2\pi j_0(p_qR_L), \tag{A.7}$$

where $j_0(z)$ is the spherical Bessel function of zeroth order. For I_3 we get,

$$I_3 = \pm\frac{1}{2}\int_0^{\pi}\mathrm{d}\theta_e\sin\theta_e\sin(p_qR_L\cos\theta_e\cos\Theta) \times\int_0^{2\pi}\mathrm{d}\phi_e\sin(p_qR_L\cos(\phi_e-\Phi)\sin\theta_e\sin\Theta), \tag{A.8}$$

being,

$$I_3 = 0, \tag{A.9}$$

as the integral in the ϕ_e variable vanishes identically. For the integral I_4, after a trivial integration over the angle ϕ_e, we find,

$$I_4 = \pi\beta\int_0^{\pi}d\theta_e\sin\theta_eP_2(\cos\theta_e) \tag{A.10}$$

$$= 0. \tag{A.11}$$

For the integral I_5 we obtain,

$$I_5 = \mp\frac{\beta}{2}\int_0^{\pi} \mathrm{d}\theta_e \sin\theta_e P_2(\cos\theta_e)\cos(p_q R_L \cos\theta_e \cos\Theta) \times \int_0^{2\pi} \mathrm{d}\phi_e \cos(p_q R_L \sin\theta_e \sin\Theta \cos(\phi_e - \Phi)), \tag{A.12}$$

where the integral over ϕ_e is solved as before to give,

$$I_5 = \mp\pi\beta\int_0^{\pi} \mathrm{d}\theta_e \sin\theta_e P_2(\cos\theta_e)\cos(p_q R_L \cos\theta_e \cos\Theta) \times J_0(p_q R_L \sin\theta_e \sin\Theta). \tag{A.13}$$

The last integral is tabulated as finite Gegenbauer integrals [45], with the result,

$$I_5 = \pm\pi\beta\sqrt{\frac{2\pi}{p_q R_L}} P_2(\cos\Theta) J_{5/2}(p_q R_L) \tag{A.14}$$

$$= \pm 2\pi\beta j_2(p_q R_L) P_2(\cos\Theta), \tag{A.15}$$

where $j_2(z)$ is the spherical Bessel function of second order. Finally, for I_6 we get,

$$I_6 = \pm\frac{\beta}{2}\int_0^{\pi} \mathrm{d}\theta_e \sin\theta_e P_2(\cos\theta_e)\sin(p_q R_L \cos\theta_e \cos\Theta) \times \int_0^{2\pi} \mathrm{d}\phi_e \sin(p_q R_L \cos(\phi_e - \Phi)\sin\theta_e \sin\Theta) \tag{A.16}$$

$$= 0, \tag{A.17}$$

as the integral over ϕ_e vanishes identically as in I_3.

References

[1] Dahlström J M, L'Huillier A and Maquet A 2012 *J. Phys. B: At. Mol. Opt. Phys.* **45** 183001
[2] Paul P M, Toma E S, Breger P, Mullot G, Aug F, Balcou P, Muller H G and Agostini P 2001 *Science* **292** 1689–92
[3] Mauritsson J, Johnsson P, Mansten E, Swoboda M, Ruchon T, L'Huillier A and Schafer K J 2008 *Phys. Rev. Lett.* **100** 073003
[4] Laurent G, Cao W, Li H, Wang Z, Ben-Itzhak I and Cocke C L 2012 *Phys. Rev. Lett.* **109** 083001
[5] Itatani J, Quéré F, Yudin G L, Ivanov M Y, Krausz F and Corkum P B 2002 *Phys. Rev. Lett.* **88** 173903
[6] Kienberger R *et al* 2004 *Nature* **427** 817–21
[7] Goulielmakis E *et al* 2004 *Science* **305** 1267–9
[8] Eckle P, Smolarski M, Schlup P, Biegert J, Staudte A, Schoffler M, Muller H G, Dorner R and Keller U 2008 *Nat Phys* **4** 565–70
[9] Meyer M *et al* 2008 *Phys. Rev. Lett.* **101** 193002
[10] Meyer M, Costello J T, Dsterer S, Li W B and Radcliffe P 2010 *J. Phys. B: At. Mol. Opt. Phys.* **43** 194006
[11] Leitner T, Taïeb R, Meyer M and Wernet P 2015 *Phys. Rev.* A **91** 063411
[12] O'Keeffe P, López-Martens R, Mauritsson J, Johansson A, L'Huillier A, Véniard V, Taïeb R, Maquet A and Meyer M 2004 *Phys. Rev.* A **69** 051401
[13] Galán A J, Argenti L and Martín F 2013 *New J. Phys.* **15** 113009
[14] Maquet A and Taïeb R 2007 *J. Mod. Opt.* **54** 1847–57
[15] Picard Y J *et al* 2014 *Phys. Rev.* A **89** 031401
[16] Yudin G L, Patchkovskii S, Corkum P B and Bandrauk A D 2007 *J. Phys. B: At. Mol. Opt. Phys.* **40** F93
[17] Yudin G L, Chelkowski S and Bandrauk A D 2006 *J. Phys. B: At. Mol. Opt. Phys.* **39** L17
[18] Boll D I R and Fojón O A 2014 *Phys. Rev.* A **90** 053414
[19] Boll D I R and Fojón O A 2016 *J. Phys. B: At. Mol. Opt. Phys.* **49** 185601
[20] Weber S J *et al* 2015 *Rev. Sci. Instrum.* **86** 033108
[21] Kazansky A K and Kabachnik N M 2007 *J. Phys. B: At. Mol. Opt. Phys.* **40** 2163
[22] Cionga A, Florescu V, Maquet A and Taïeb R 1993 *Phys. Rev.* A **47** 1830–40
[23] Zhang C H and Thumm U 2010 *Phys. Rev.* A **82** 043405
[24] Lee H C, Jheng S D and Jiang T F 2012 *J. Opt. Soc. Am.* B **29** 286–93
[25] Cohen H D and Fano U 1966 *Phys. Rev.* **150** 30–3
[26] Walter M and Briggs J 1999 *J. Phys. B: At. Mol. Opt. Phys.* **32** 2487
[27] Weck P, Fojón O A, Hanssen J, Joulakian B and Rivarola R D 2001 *Phys. Rev.* A **63** 042709
[28] Ciappina M F, Fojón O A and Rivarola R D 2014 *J. Phys. B: At. Mol. Opt. Phys.* **47** 042001
[29] Lein M, Hay N, Velotta R, Marangos J P and Knight P L 2002 *Phys. Rev.* A **66** 023805
[30] Itatani J, Levesque J, Zeidler D, Niikura H, Pepin H, Kieffer J C, Corkum P B and Villeneuve D M 2004 *Nature* **432** 867–71
[31] Kanai T, Minemoto S and Sakai H 2005 *Nature* **435** 470–4
[32] Vozzi C *et al* 2005 *Phys. Rev. Lett.* **95** 153902
[33] Vozzi C *et al* 2006 *J. Phys. B: At. Mol. Opt. Phys.* **39** S457
[34] Cooper J and Zare R N 1968 *J. Chem. Phys.* **48** 942–3
[35] Mauritsson J, Gaarde M B and Schafer K J 2005 *Phys. Rev.* A **72** 013401
[36] Huang K N, Johnson W and Cheng K 1981 *At. Data Nucl. Data Tables* **26** 33–45
[37] Boll D I R and Fojón O A 2017 *J. Phys. B: At. Mol. Opt. Phys.* **50** 055604
[38] Yudin G L, Patchkovskii S and Bandrauk A D 2008 *J. Phys. B: At. Mol. Opt. Phys.* **41** 045602
[39] Dill D 1976 *J. Chem. Phys.* **65** 1130–3
[40] Yang C N 1948 *Phys. Rev.* **74** 764–72
[41] Reid K L 2003 *Annu. Rev. Phys. Chem.* **54** 397–424
[42] Fojón O A, Fernández J, Palacios A, Rivarola R D and Martín F 2004 *J. Phys. B: At. Mol. Opt. Phys.* **37** 3035
[43] Fernández J, Fojón O, Palacios A and Martín F 2007 *Phys. Rev. Lett.* **98** 043005
[44] Gradshteyn I S and Ryzhik I M 2007 *Table of Integrals, Series, and Products* 7th edn (Amsterdam: Elsevier/Academic Press)
[45] Watson G N 1944 *A Treatise on the Theory of Bessel Functions* (Cambridge: Cambridge University Press)